Supplemental Material - Electric Field Induced Associations in the Double Layer of Salt-in-Ionic-Liquid Electrolytes

Daniel M. Markiewitz,[1] Zachary A. H. Goodwin,[2,3] Michael McEldrew,[1] J. Pedro de Souza,[1,4] Xuhui Zhang,[5] Rosa M. Espinosa-Marzal,[5,6] and Martin Z. Bazant[1,7,*]

[1]*Department of Chemical Engineering, Massachusetts Institute of Technology, Cambridge, Massachusetts 02139, USA*

[2]*John A. Paulson School of Engineering and Applied Sciences, Harvard University, Cambridge, Massachusetts 02138, United States*

[3]*Departments of Materials, Imperial College London, South Kensington Campus, London SW7 2AZ, UK*

[4]*Omenn-Darling Bioengineering Institute, Princeton University, Princeton, New Jersey 08544, USA*

[5]*Department of Civil and Environmental Engineering, University of Illinois at Urbana–Champaign, Urbana, IL, 61801 USA*

[6]*Department of Materials Science and Engineering, University of Illinois at Urbana–Champaign, Urbana, IL, 61801 USA*

[7]*Department of Mathematics, Massachusetts Institute of Technology, Cambridge, Massachusetts 02139, USA*

(Dated: July 16, 2024)

* e-mail: bazant@mit.edu

I. MODEL PREDICTIONS FOR ALTERNATIVE PARAMETERS

In the main text, the analysis centered around parameters that were extracted from MD simulations and in the pre-gel regime where we could access its predictions [1]. Extending this model into the post-gel regime follows a similar framework as with previous works, with the additional change of expanding upon the regular solution interaction term to be capable of capturing the effects of having gel-species [1, 2]. A sample of alternative parameter choices are presented here to better demonstrate the underlying physics that this model may predict and discuss briefly the basis behind why the various changes in electrolyte behavior arise.

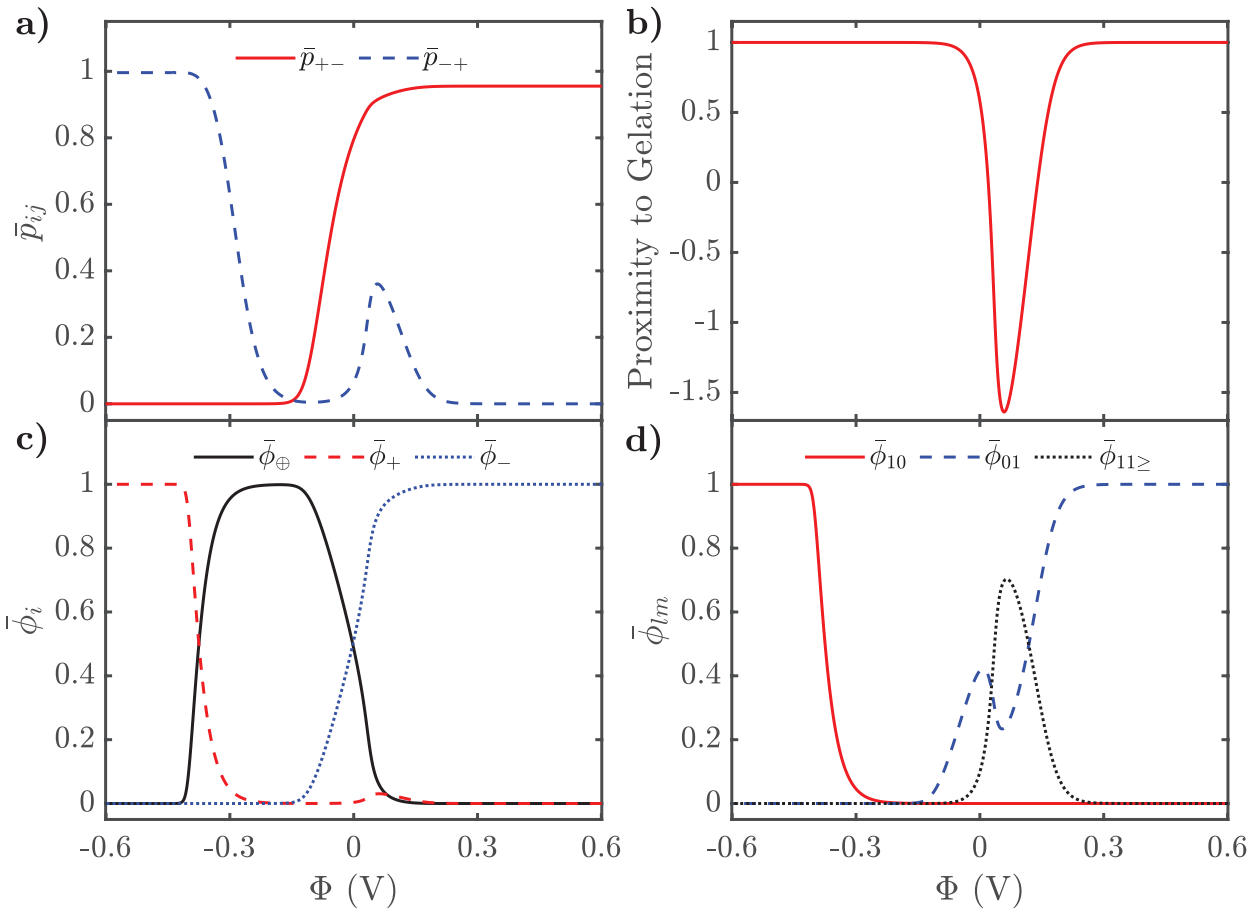

FIG. S1. Properties of the EDL of SiILs at a higher mole fraction of alkali metal salt as a function of applied electrostatic potential. a) Association probabilities. b) Proximity to gelation, $1 - \bar{p}_{+-}\bar{p}_{-+}(f_+ - 1)(f_- - 1)$. c) Total volume fractions of each species. d) Volume fraction of free cations, anions and clusters. Here we use $x_s = 0.05$, $f_+ = 5$, $f_- = 3$, $\xi_+ = 1$, $\xi_- = 7$, $\xi_\oplus = 7$, $\chi = -2$ k_BT, and $\lambda_0 = 50$. Here we observe that sufficiently high mole fractions of alkali metal salt lead to a local minimum in the free IL anions emerging around low positive potentials. Besides the formation of a local minimum from the increased presence of alkali metal salt, the predictions of this electrolytes composition in the EDL does not depart drastically from the case discussed in the main paper. This increased presence also leads to a decrease in the voltage plateau before the cation exchange occurs. The influence of gelation is ignored naively for the current study; therefore, more nuanced differences may result if the influence of gelation is significant. Note we observe gel from 0.020 V to 0.140 V.

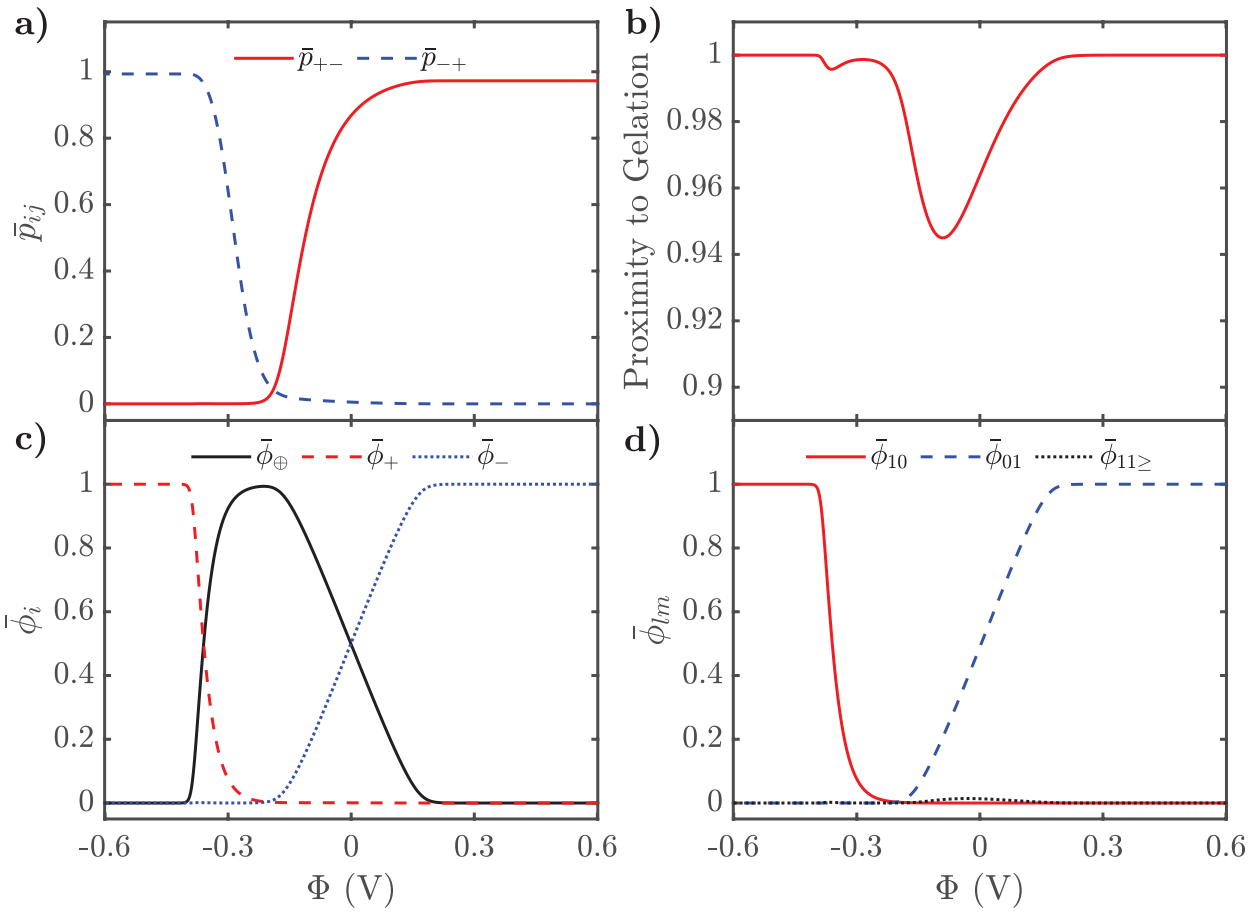

FIG. S2. Properties of the EDL of SiILs with flipped functionalities as a function of applied electrostatic potential. a) Association probabilities. b) Proximity to gelation, $1-\bar{p}_{+-}\bar{p}_{-+}(f_+-1)(f_--1)$. c) Total volume fractions of each species. d) Volume fraction of free cations, anions and clusters. Here we use $x_s = 0.01$, $f_+ = 3$, $f_- = 5$, $\xi_+ = 1$, $\xi_- = 7$, $\xi_\oplus = 7$, $\chi = -2\ \mathrm{k}_B\mathrm{T}$, and $\lambda_0 = 50$. Here we see a deviation in the predictions of the SiILs properties compared to the main case. The decrease of the bulk's proximity to gelation is expected from the composition of the SiIL. From this decrease, the increase in aggregation is seen at modest applied negative potentials. Beyond this, we observe the voltage plateau shrinks. We note that a secondary increase in aggregation occurs after the voltage plateau. This effect helps highlight the role of the regular solution interactions in the fluctuation of aggregation in the EDL. This change leads to the enhancement of aggregation occurring at a modest applied negative potentials, as well as secondary enhancement in aggregation emerging at higher but not extreme applied negative potentials. The nuanced interplay of the SiIL parameters can lead to the secondary enhancement being larger than the first enhancement as well as shifting the enhancements to different voltages.

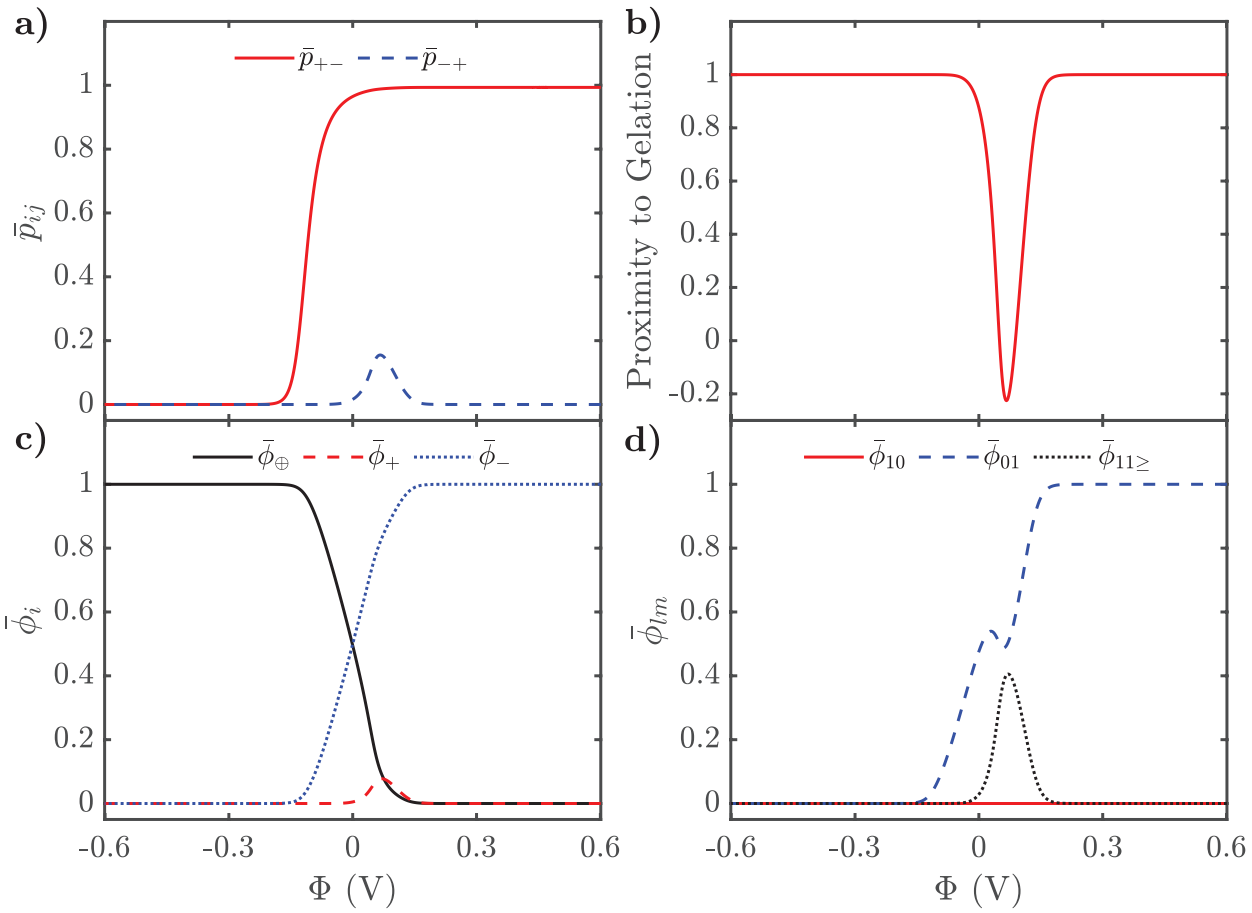

FIG. S3. Properties of the EDL of SiILs with equal sized species as a function of applied electrostatic potential. a) Association probabilities. b) Proximity to gelation, $1-\bar{p}_{+-}\bar{p}_{-+}(f_+-1)(f_--1)$. c) Total volume fractions of each species. d) Volume fraction of free cations, anions and clusters. Here we use $x_s = 0.01$, $f_+ = 5$, $f_- = 3$, $\xi_+ = \xi_- = \xi_\oplus = 1$, $\chi = -2$ k_BT, and $\lambda_0 = 50$. We observe that the bulk system initially is closer to gelation and obtains a similar enhancement at small positive potentials as before. The system here enters the post-gel regime; however, more nuanced effects may not be captured as previously discussed. Additionally unlike in the main case, we do not see the cation exchange occurring in our system even for large negative potentials. This finding is expected as the alkali metal cation no longer has a larger charge density. Lastly, we can note the alkali metal cation enhancement as seen in c), which is harder to observe in the main case, given the significant size difference between the species. Note we observe gel from 0.050 V to 0.088 V.

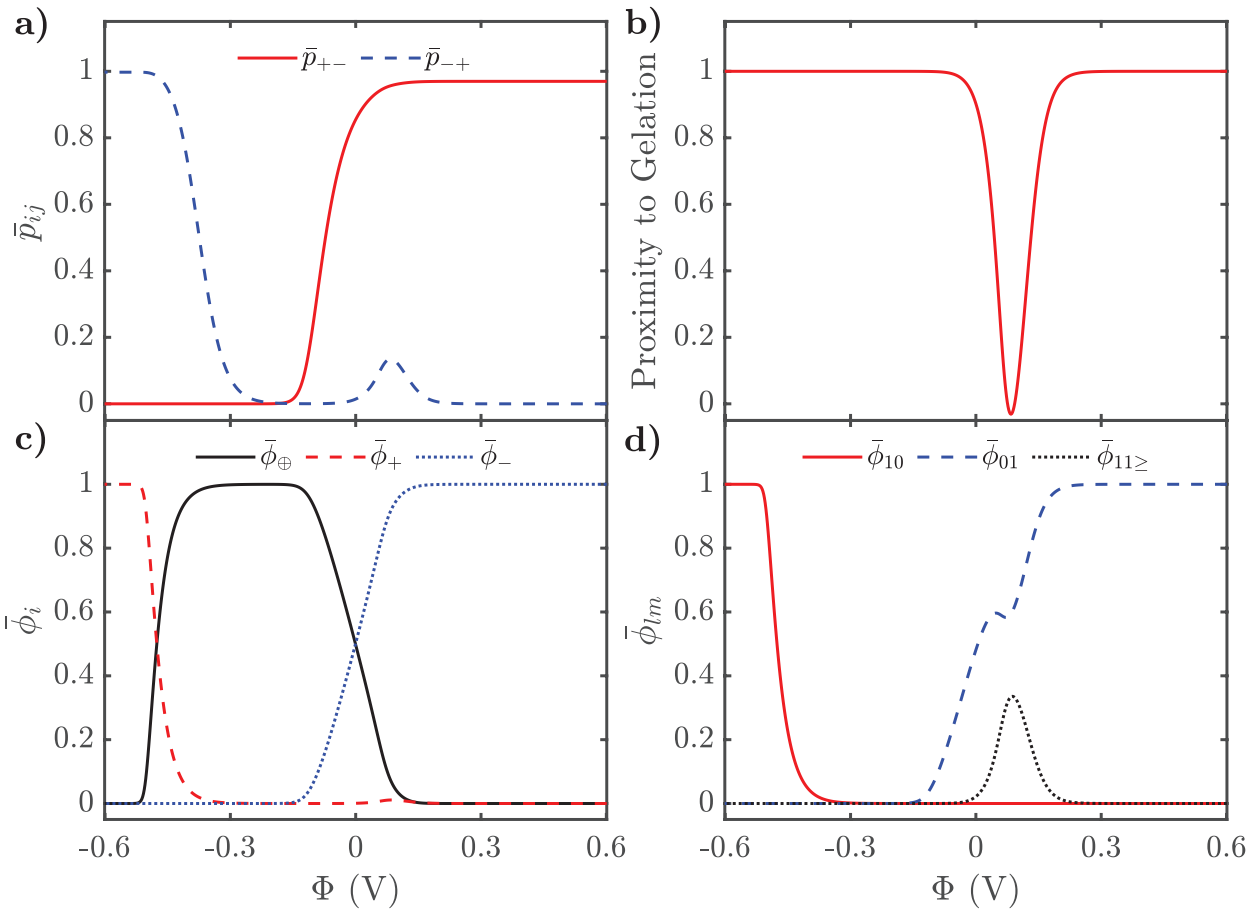

FIG. S4. Properties of the EDL of SiILs with a stronger "bare" association constant, λ_0, as a function of applied electrostatic potential. a) Association probabilities. b) Proximity to gelation, $1 - \bar{p}_{+-}\bar{p}_{-+}(f_+ - 1)(f_- - 1)$. c) Total volume fractions of each species. d) Volume fraction of free cations, anions and clusters. We use $x_s = 0.01$, $f_+ = 5$, $f_- = 3$, $\xi_+ = 1$, $\xi_- = 7$, $\xi_\oplus = 7$, $\chi = -2$ k_BT, and $\lambda_0 = 75$. Here we see that the bulk gets closer to gelation. This change leads to a similar prediction in regards to the enhancement of aggregations at modest applied positive potentials that is seen when the mole fraction of alkali metal salt was increased. Uniquely here, the voltage plateau expands, which differs from the voltage plateau contraction seen with an increased mole fraction of alkali metal salt. This expansion comes primarily from decreasing the favorability of the associating species being brought into the EDL. Note we observe gel from 0.076 V to 0.093 V.

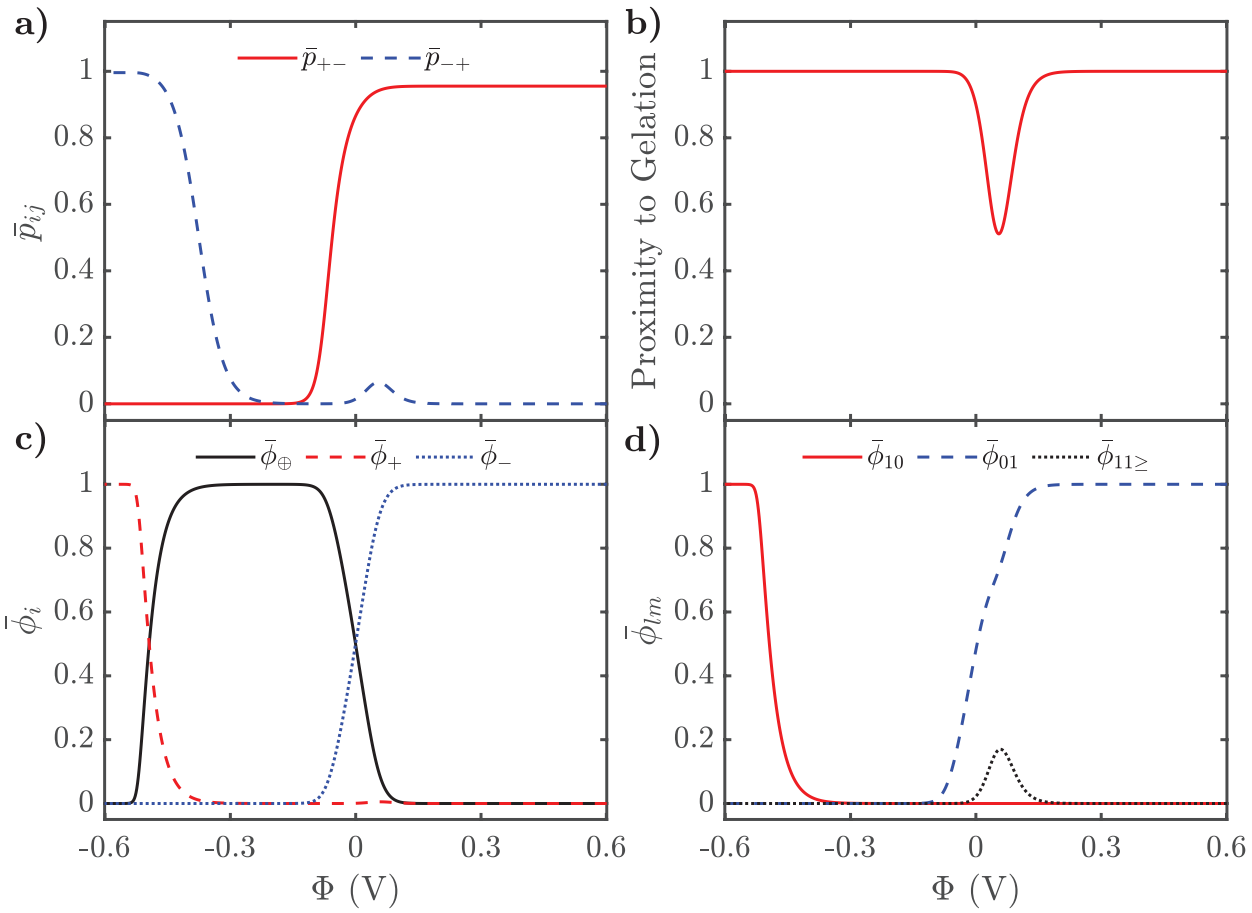

FIG. S5. Properties of the EDL of SiILs with a weaker regular solution interaction strength, χ, as a function of applied electrostatic potential. a) Association probabilities. b) Proximity to gelation, $1 - \bar{p}_{+-}\bar{p}_{-+}(f_+ - 1)(f_- - 1)$. c) Total volume fractions of each species. d) Volume fraction of free cations, anions and clusters. Here we use $x_s = 0.01$, $f_+ = 5$, $f_- = 3$, $\xi_+ = 1$, $\xi_- = 7$, $\xi_{\oplus} = 7$, $\chi = -1$ $k_B T$, and $\lambda_0 = 50$. Here the enhancement of aggregates at low positive potentials decreases. This weaker regular solution interaction strength also leads to an expanded voltage plateau before the cation exchange occurs, as compared to the main case. This effect comes from the impact of having weaker regular solution interactions, meaning it's less able to compensate for the unfavorability of bringing the associating species into the EDL.

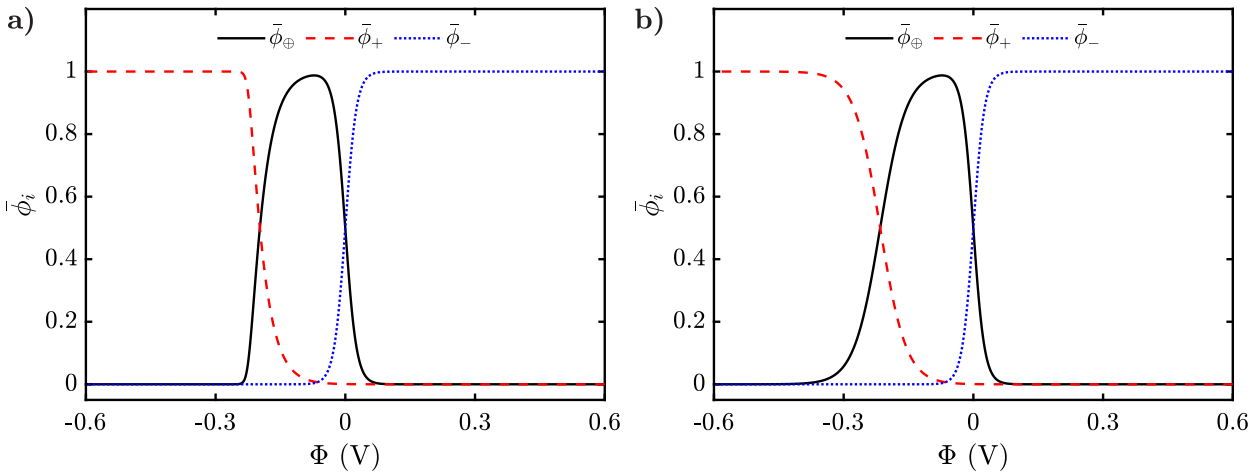

FIG. S6. Total volume fractions of each species in EDL of SiILs without associations and regular solution interactions as a function of applied electrostatic potential. a) Incompressible model. b) Asymmetric 3-component Langmuir model [3]. Here we use $x_s = 0.01$, $\xi_+ = 1$, $\xi_- = 7$, and $\xi_\oplus = 7$ for both models. Here one can observe the cation exchange at lower electric potentials than in the main case, occurring at -0.20 V for the Incompressible model and -0.22 V for the Asymmetric 3-component Langmuir model. This exchange is driven by the difference in the charge density between the cations as well as the bulk composition of the electrolyte solution.

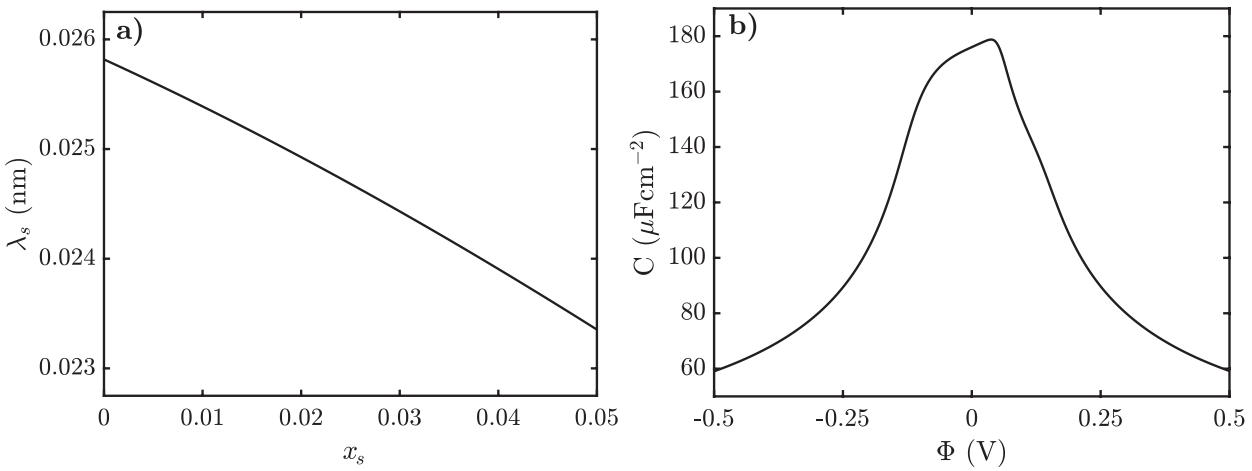

FIG. S7. a) Screening length of SiIL with equal sized species as a function of the mole fraction of alkali metal salt. b) Differential capacitance of SiIL with equal sized species and $x_s = 0.01$, as a function of electrostatic potential. Here we use $f_+ = 5$, $f_- = 3$, ξ_+=ξ_-=$\xi_\oplus$=1, $\chi = -2$ k_BT, $\lambda_0 = 50$, and $\epsilon_r = 5$. a) We see here that the screening length is decreased significantly compared to the case seen in the main paper. This drop across the mole fraction of alkali metal salt points towards the dominant role the formation of aggregates have on the screening length. b) We can note that the satellite peak associated with the cation exchange disappears. This change follows from the fact that there is now no difference in the charge density of our cations which leads to no cation exchange. Here, we can also see more prominently the effects of the induced associations at modest positive potentials via the low potential differential capacitance peak being even larger. Additionally, we observe that at low magnitudes of potential that the differential capacitance decays asymmetrically before returning to similar rates of decay at larger magnitudes of potential. After 0.050 V we would expect gel to be present in some parts of the EDL.

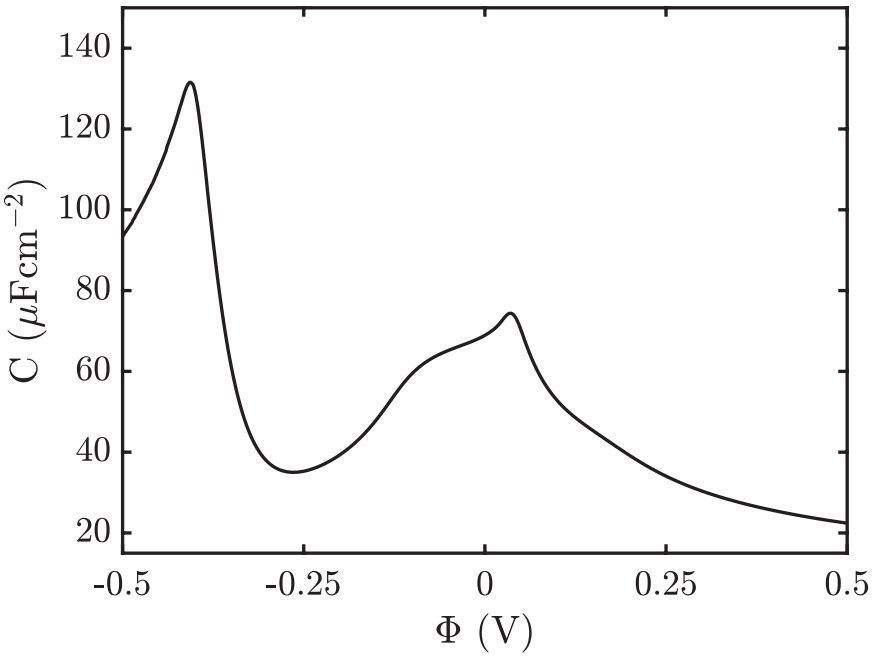

FIG. S8. Differential capacitance of SiIL at a higher mole fraction of alkali metal salt as a function of electrostatic potential. Here we use $x_s = 0.05$, $f_+ = 5$, $f_- = 3$, $\xi_+ = 1$, $\xi_- = 7$, $\xi_\oplus = 7$, $\chi = -2$ k$_B$T, $\lambda_0 = 50$, and $\epsilon_r = 5$. Here we can observe that the induced associations are even more enhanced at modest positive potentials, which appears to make the low potential differential capacitance peak even larger. Additionally, we can note as potentials increase that the decay is asymmetric and steeper initially for the positive potentials. Once again, we see the secondary satellite peak associated with the cation exchange. After 0.020 V we would expect gel to be present in some parts of the EDL.

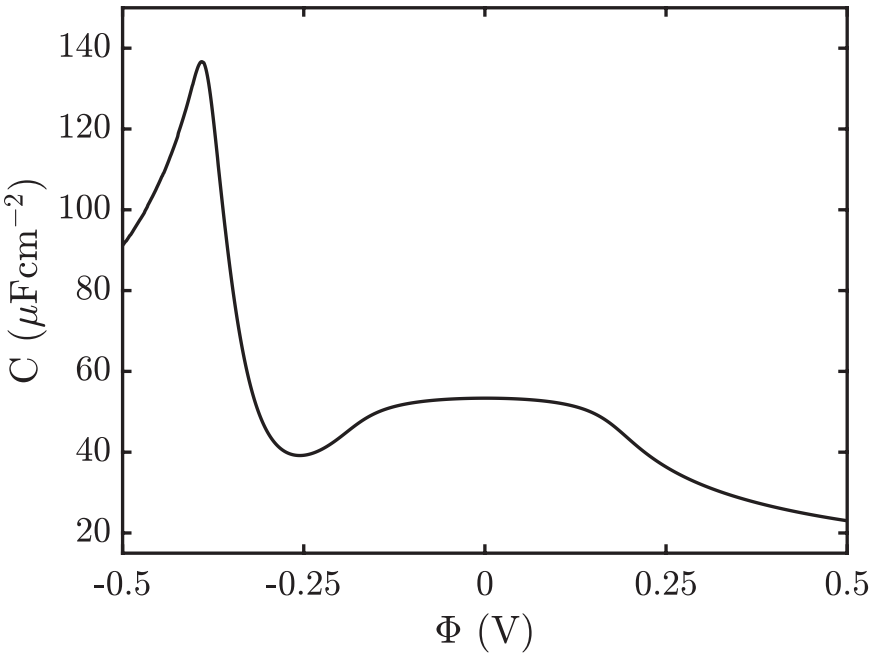

FIG. S9. Differential capacitance of SiIL with flipped functionalities as a function of electrostatic potential. Here we use $x_s = 0.01$, $f_+ = 3$, $f_- = 5$, $\xi_+ = 1$, $\xi_- = 7$, $\xi_\oplus = 7$, $\chi = -2$ k$_B$T, $\lambda_0 = 50$, and $\epsilon_r = 5$. Here we can observe that the initial bell shape is elongated. This influence may be due to the induced associations now occurring at modest negative potentials. Once again, we note the secondary satellite peak associated with the cation exchange.

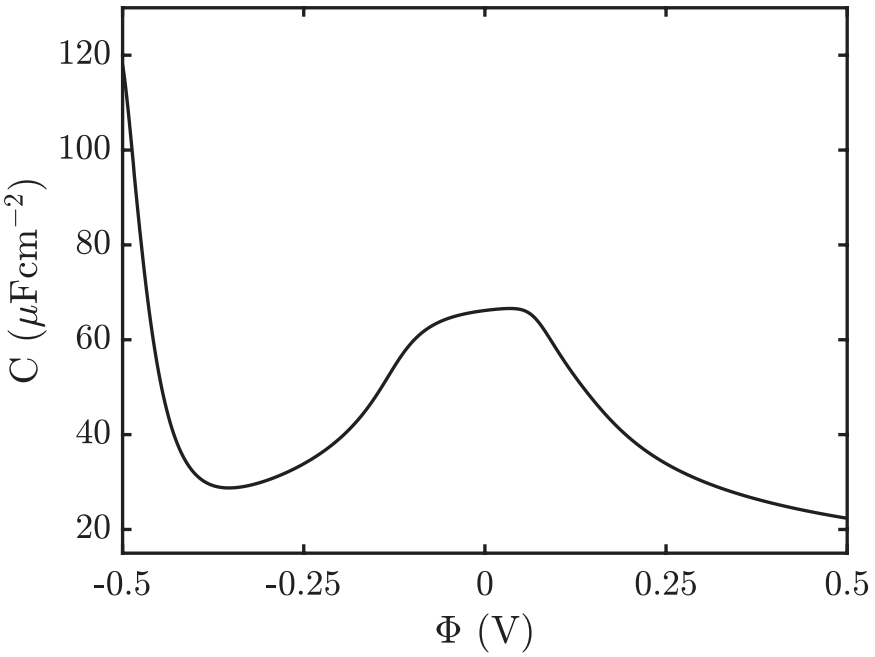

FIG. S10. Differential capacitance of SiIL with a stronger "bare" association constant, λ_0, as a function of electrostatic potential. Here we use $x_s = 0.01$, $f_+ = 5$, $f_- = 3$, $\xi_+ = 1$, $\xi_- = 7$, $\xi_\oplus = 7$, $\chi = -2$ k$_B$T, $\lambda_0 = 75$, and $\epsilon_r = 5$. We can observe that the secondary satellite peak associated with the cation exchanges emerges at even larger negative voltages. This is expected as a stronger "bare" association constant increases the width of the voltage plateau. Additionally, the induced associations at modest positive potentials are further enhanced making the low potential differential capacitance peak even larger than the main case. After 0.076 V we would expect gel to be present in some parts of the EDL.

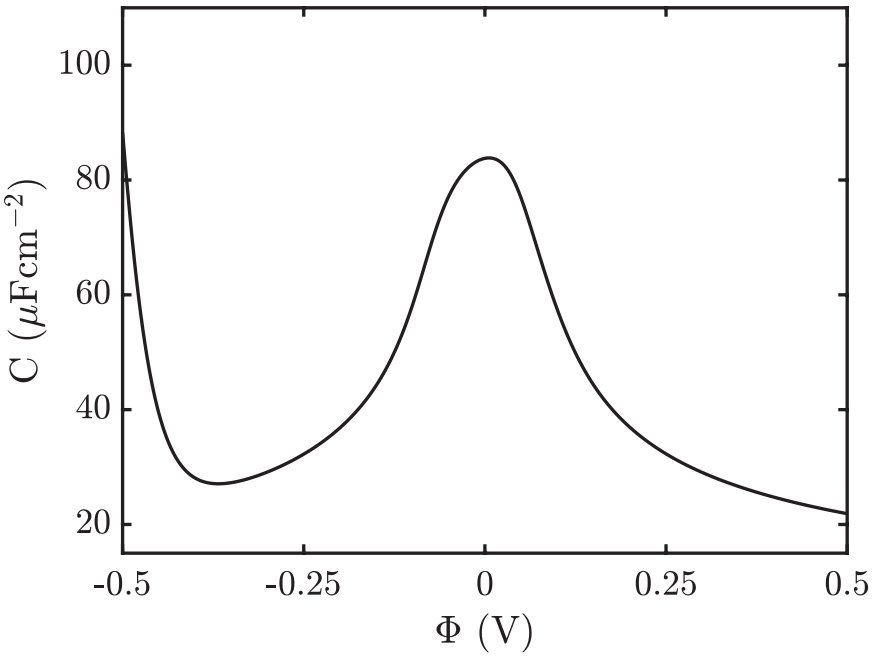

FIG. S11. Differential capacitance of SiIL with a weaker regular solution interaction strength, χ, as a function of electrostatic potential. Here we use $x_s = 0.01$, $f_+ = 5$, $f_- = 3$, $\xi_+ = 1$, $\xi_- = 7$, $\xi_\oplus = 7$, $\chi = -1$ k$_B$T, $\lambda_0 = 50$, and $\epsilon_r = 5$. The secondary satellite peak associated with the cation exchanges emerges once again at an even higher voltage than the main case. This change is expected as a weaker regular solution interaction strength increases the width of the voltage plateau. Additionally we observe, as shown in Fig. S5, a decrease in the enhancement of aggregations at low positive potentials. This decrease appears to make the low potential differential capacitance peak significantly less prominent than the main case.

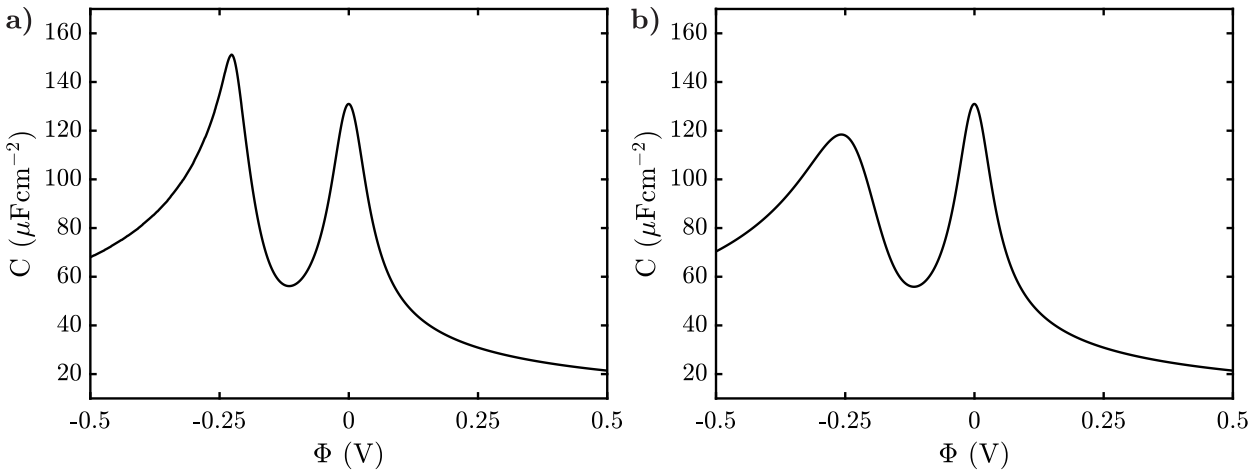

FIG. S12. Differential capacitance of SiIL without associations and regular solution interactions as a function of electrostatic potential. a) Incompressible model. b) Asymmetric 3-component Langmuir model [3]. Here we use $x_s = 0.01$, $\xi_+ = 1$, $\xi_- = 7$, and $\xi_\oplus = 7$ for both models. Here we can observe that the initial bell shape is much sharper in both cases compared to the main case. This influence may be due to the lack of associations and regular solution interactions compressing the initial bell shape. We can note that the secondary satellite peak associated with the cation exchange occurs in both models.

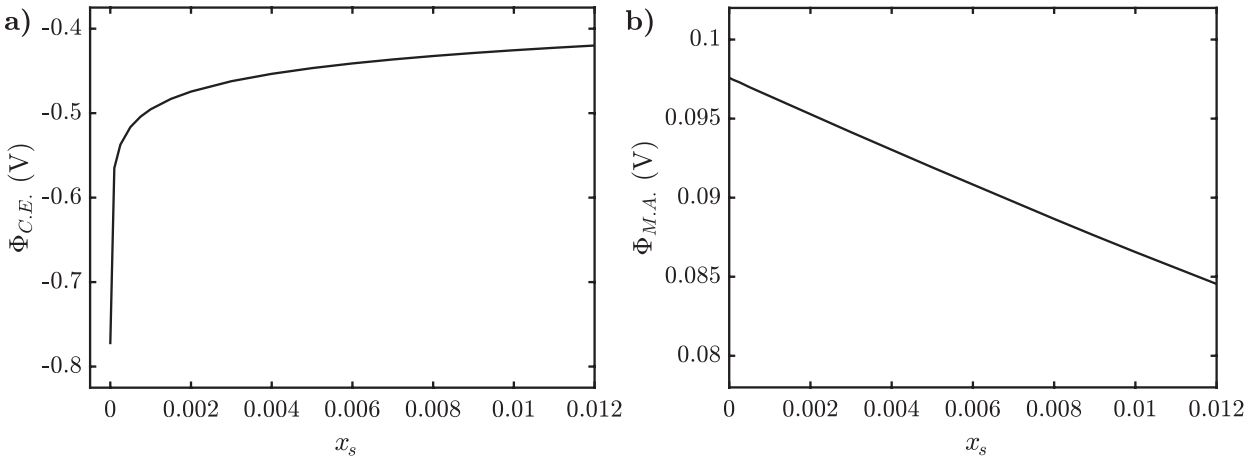

FIG. S13. Voltage trends of SiIL as a function of the mole fraction of alkali metal salt. a) Cation exchange voltage. b) Maximum aggregation voltage. Here we use $f_+ = 5$, $f_- = 3$, $\xi_+ = 1$, $\xi_- = 7$, $\xi_\oplus = 7$, $\chi = -2$ k$_B$T, and $\lambda_0 = 50$. a) Note as the mole faction of alkali metal salt goes to zero the cation exchange voltage diverges and at zero it does not exist. b) Note the maximum aggregation voltage also does not exist at zero.

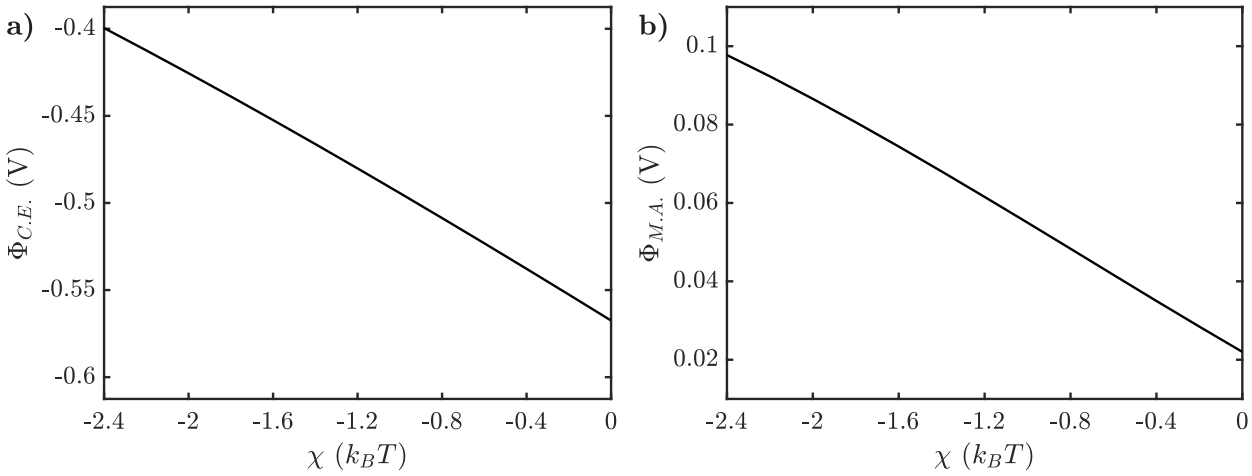

FIG. S14. Voltage trends of SiIL as a function of the regular solution interaction strength, χ. a) Cation exchange voltage. b) Maximum aggregation voltage. Here we use $x_s = 0.01$, $f_+ = 5$, $f_- = 3$, $\xi_+ = 1$, $\xi_- = 7$, $\xi_\oplus = 7$, and $\lambda_0 = 50$.

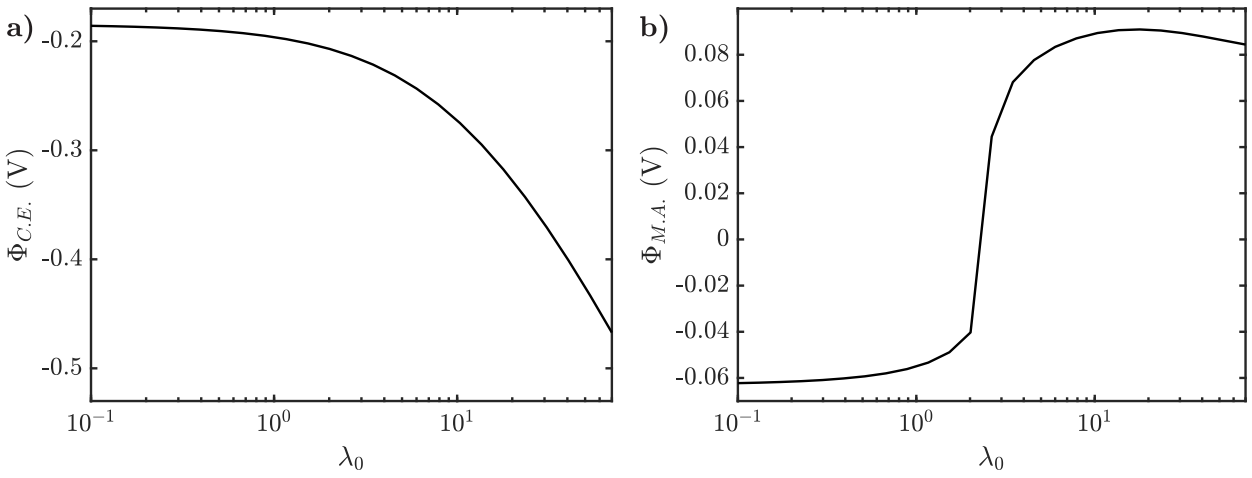

FIG. S15. Voltage trends of SiIL as a function of the "bare" association constant, λ_0. a) Cation exchange voltage. b) Maximum aggregation voltage. Here we use $x_s = 0.01$, $f_+ = 5$, $f_- = 3$, $\xi_+ = 1$, $\xi_- = 7$, $\xi_\oplus = 7$, and $\chi = -2$ k_BT.

II. NOTES ON SYSTEM OF EQUATIONS AND CALCULATIONS

In this section we highlight the system of equations used, how they can be implemented, and how to utilize them to reproduce the calculations shown in the main text and supplemental material.

A. System of Equations

As discussed in the main text we arrive at the following set of 6 equations:

$$\begin{aligned}
\bar{\phi}_{10} &= \phi_{10}\exp(-e\beta\Phi+\Lambda)\\
\bar{\phi}_{01} &= \phi_{01}\exp(e\beta\Phi-\beta\chi f_{-}(\bar{\phi}_{\oplus}-\phi_{\oplus})+\xi_{-}\Lambda)\\
\bar{\phi}_{\oplus} &= \phi_{\oplus}\exp\left(-e\beta\Phi+\beta\chi f_{-}\xi_{\oplus}\left\{c_{-}(1-p_{-+})-\bar{c}_{-}(1-\bar{p}_{-+})\right\}+\xi_{\oplus}\Lambda\right)\\
\bar{\phi}_{+}+\bar{\phi}_{-}+\bar{\phi}_{\oplus} &= 1\\
\psi_{+}p_{+-} &= \frac{1+\lambda(\psi_{-}+\psi_{+})-\sqrt{\left[1+\lambda(\psi_{-}+\psi_{+})\right]^{2}-4\lambda^{2}\psi_{-}\psi_{+}}}{2\lambda}\\
\psi_{-}p_{-+} &= \frac{1+\lambda(\psi_{-}+\psi_{+})-\sqrt{\left[1+\lambda(\psi_{-}+\psi_{+})\right]^{2}-4\lambda^{2}\psi_{-}\psi_{+}}}{2\lambda}
\end{aligned}$$

We convert reduce this system of equations to only depend on ($\bar{\phi}_{+}$,$\bar{\phi}_{-}$,$\bar{\phi}_{\oplus}$,$\bar{p}_{+-}$,$\bar{p}_{-+}$,Λ) by asserting $\phi_{10}=\phi_{+}(1-p_{+-})^{f_{+}}$ and $\phi_{01}=\phi_{-}(1-p_{-+})^{f_{-}}$ as mentioned in the main text. From this we obtain the following system of equations,

$$\begin{aligned}
\bar{\phi}_{+} &= \frac{\phi_{10}}{(1-\bar{p}_{+-})^{f_{+}}}\exp(-e\beta\Phi+\Lambda)\\
\bar{\phi}_{-} &= \frac{\phi_{01}}{(1-\bar{p}_{-+})^{f_{-}}}\exp(e\beta\Phi-\beta\chi f_{-}(\bar{\phi}_{\oplus}-\phi_{\oplus})+\xi_{-}\Lambda)\\
\bar{\phi}_{\oplus} &= \phi_{\oplus}\exp\left(-e\beta\Phi+\beta\chi f_{-}\xi_{\oplus}\left\{c_{-}(1-p_{-+})-\bar{c}_{-}(1-\bar{p}_{-+})\right\}+\xi_{\oplus}\Lambda\right)\\
\bar{\phi}_{+}+\bar{\phi}_{-}+\bar{\phi}_{\oplus} &= 1\\
\psi_{+}p_{+-} &= \frac{1+\lambda(\psi_{-}+\psi_{+})-\sqrt{\left[1+\lambda(\psi_{-}+\psi_{+})\right]^{2}-4\lambda^{2}\psi_{-}\psi_{+}}}{2\lambda}\\
\psi_{-}p_{-+} &= \frac{1+\lambda(\psi_{-}+\psi_{+})-\sqrt{\left[1+\lambda(\psi_{-}+\psi_{+})\right]^{2}-4\lambda^{2}\psi_{-}\psi_{+}}}{2\lambda}
\end{aligned}$$

where the last three equations hold for both the EDL and bulk quantities. Other formulations and manipulations of this system of equations can be constructed and are equivalent to the one presented here so long as the alternative system of equations satisfy the original equations presented in the main text. With this and the bulk quantities calculated, as discussed in the main text, one can implement them into a numerical solver to obtain values for ($\bar{\phi}_+$,$\bar{\phi}_-$,$\bar{\phi}_\oplus$,$\bar{p}_{+-}$,$\bar{p}_{-+}$,Λ) at a given electrostatic potential (Φ) and bulk properties (ϕ_+,ϕ_-,$\phi_\oplus$,λ_0,χ).

B. EDL Calculations

To solve for profiles in the EDL as well as the differential capacitance, screening length, cation exchange voltage and maximum aggregation voltage, we use the following steps:

1. First, we solve the our system of equations numerically for $\bar{\phi}_+$,$\bar{\phi}_-$,$\bar{\phi}_\oplus$,$\bar{p}_{+-}$,$\bar{p}_{-+}$,Λ over a range of electrostatic potential values. This is done for a spectrum of dimensionless electrostatic potential ($e\beta\Phi$) to allow one to create a sufficiently fine grid, for our purposes here a spacing of 0.001 was used. Here to simplify further steps, we stored the resulting fine maps for $\bar{\phi}_+$,$\bar{\phi}_-$,$\bar{\phi}_\oplus$,$\bar{p}_{+-}$,$\bar{p}_{-+}$,Λ, and dimensionless ρ_e, allowing for one to interpolated solutions to these quantities for a given electrostatic potential.

2. Using the dimensionless ρ_e map, we can then numerically solve the Poisson-Boltzmann equation to get a solution for the electrostatic potential profile in the EDL.

3. The electrostatic potential profile in the EDL along with our interpolation maps allows us to predict profiles of the various quantities of interest in the EDL: dimensionless charge density, total volume fractions of each species, volume fraction of free cations, volume fraction free anions, volume fraction aggregates (could additional extract individual clusters volume fractions), association probabilities, and the product of association probabilities.

4. In order to obtain our differential capacitance predictions, we first solved for the potential at the interface using a wide range of surface charge densities for our boundary conditions, for our work here we used a fine grid spacing of 0.0001 C/m^2. From this map, we constructed splines to calculate how the surface charge density depends on

the potential at the interface. Using this we were able to calculate the differential capacitance numerically using finite differences.

5. To obtain the screening length, we next applied a ± 0.0001 V electrostatic potential boundary condition at the surface. From the electrostatic potential profile in the EDL, we obtained the screening length by fitting the exponential decay for the profile, thus extracting the exponential decay constant for a range of mole fractions of alkali metal salt shown in Fig. 5.a). In Fig. 5.a) it was constructed using a -0.0001 V electrostatic potential boundary condition. It is worth noting that the screening lengths obtained by ± 0.0001 V solutions are very similar. Additionally for the screening length plot in Fig. 5.a) and Fig. S7.a) these profiles are within the pre-gel regime.

6. The cation exchange voltage and maximum aggregation voltage utilized the method in step 1. For these plots, we utilize the values for the case displayed in the main text but individually varied the values of the mole fraction of alkali metal salt (x_s), regular solution interaction strength (χ), and "bare" association constant (λ_0) extracting the cation exchange voltage and maximum aggregation voltage for each case. For the cation exchange voltage plot shown here, we numerically solve for the larger negative voltage at which the spline fitted $\bar{\phi}_{\oplus}$ and $\bar{\phi}_{+}$ were equal. There can also be a second voltage at a smaller magnitude where they equal. For the voltage at the maximum aggregation, we extracted it directly by finding the minimum of the proximity of gelation.

[1] M. McEldrew, Z. A. H. Goodwin, N. Molinari, B. Kozinsky, A. A. Kornyshev, and M. Z. Bazant, J. Phys. Chem. B **125**, 13752 (2021).

[2] M. McEldrew, Z. A. Goodwin, S. Bi, M. Z. Bazant, and A. A. Kornyshev, J. Chem. Phys. **152**, 234506 (2020).

[3] M. McEldrew, Z. A. Goodwin, A. A. Kornyshev, and M. Z. Bazant, The journal of physical chemistry letters **9**, 5840 (2018).